

# Nanoscale

Accepted Manuscript



This is an *Accepted Manuscript*, which has been through the Royal Society of Chemistry peer review process and has been accepted for publication.

*Accepted Manuscripts* are published online shortly after acceptance, before technical editing, formatting and proof reading. Using this free service, authors can make their results available to the community, in citable form, before we publish the edited article. We will replace this *Accepted Manuscript* with the edited and formatted *Advance Article* as soon as it is available.

You can find more information about *Accepted Manuscripts* in the [Information for Authors](#).

Please note that technical editing may introduce minor changes to the text and/or graphics, which may alter content. The journal's standard [Terms & Conditions](#) and the [Ethical guidelines](#) still apply. In no event shall the Royal Society of Chemistry be held responsible for any errors or omissions in this *Accepted Manuscript* or any consequences arising from the use of any information it contains.



## Fabrication and optical enhancing properties of discrete supercrystals

Received 00th January 20xx,  
Accepted 00th January 20xx

DOI: 10.1039/x0xx00000x

[www.rsc.org/](http://www.rsc.org/)

Moritz Tebbe,<sup>a</sup> Sarah Lentz,<sup>a</sup> Luca Guerrini,<sup>b</sup> Andreas Fery,<sup>\*a,c</sup> Ramon A. Alvarez-Puebla<sup>\*b,d,e</sup> and Nicolas Pazos-Perez<sup>\*a,b,d</sup>

Discrete gold nanoparticle crystals with tunable size and morphology are fabricated via a fast, inexpensive template-assisted method. The highly precise hierarchical organization of the plasmonic building blocks yields superstructures with outstanding behaviour for surface-enhanced Raman scattering analysis.

### Introduction

Surface structuration consists of organizing hierarchical structures where a unit cell with micro- or nano-scale dimensions is repeated over macroscopic length scales.<sup>1</sup> Such structuration can lead to a broad range of functionalities that can be harnessed to introduce specific optical properties,<sup>1-4</sup> controlled wetting response,<sup>5-7</sup> self-cleaning ability<sup>8, 9</sup> or antireflective<sup>10</sup> and catalytic features.<sup>11, 12</sup> All these functionalities solely arise from the specific surface structuration. For this reason, the controlled production of macroscopic materials with micro- and nano-structured features is a focus of increasing interest in current multidisciplinary research.

Usually, the fabrication of controlled structures requires the use of advanced top-down methods like electron- or ion-beam lithography.<sup>13, 14</sup> Unfortunately, these techniques are expensive, time-consuming and cannot be scaled or parallelized. To overcome these issues, bottom-up approaches based on self-assembly of colloidal particles<sup>15, 16</sup> were developed as a promising alternative for the formation of organized assemblies on large areas.<sup>17-22</sup> Furthermore, the use of nanoparticles (NPs) as building blocks to form three-dimensional superlattices (i.e. supercrystals) offers the possibility to implement in the material extra properties arising from the specific NP interactions. Such additional features can be rationally tuned by manipulating the size,

shape and composition of the NPs. In particular, interparticle interactions can lead to collective properties which are significantly different from those of the isolated NPs.<sup>23</sup> Therefore, this type of supercrystals is emerging as a new and important class of nanostructured materials that are suited for a number of applications from photonics<sup>3, 17, 19, 24-28</sup> to energy storage and production.<sup>29, 30</sup> Despite many examples reported in the literature, most of fabrication methods rely on the production of continuous crystals<sup>17, 31</sup> while only few describe the production of nanostructured surfaces from individual supercrystals.<sup>32-35</sup> This is mainly due to the limited control that can be exercised on the self-assembly of colloidal NPs resulting from the broad set of different factors and driving forces (i.e. van der Waals, coulombic, dipolar, entropic, capillary, convective, shear etc.) involved in the particle-particle and particle-substrate interactions.<sup>36</sup> As a result, the optical properties of these materials, and especially those formed of plasmonic NPs, are only partially characterized. Here we report a fast and inexpensive template-assisted method to form discrete colloidal crystals (i.e. supercrystals) over large areas, based on the confined sedimentation, and subsequent drying of colloidal particles. The obtained materials are characterized by means of surface-enhanced Raman scattering (SERS) mapping in order to define their optical enhancing properties.

### Experimental section

<sup>a</sup> Department of Physical Chemistry II, University of Bayreuth Universitaetsstrasse 30, Bayreuth 95440, Germany. Email: [fery@ipfdd.de](mailto:fery@ipfdd.de)

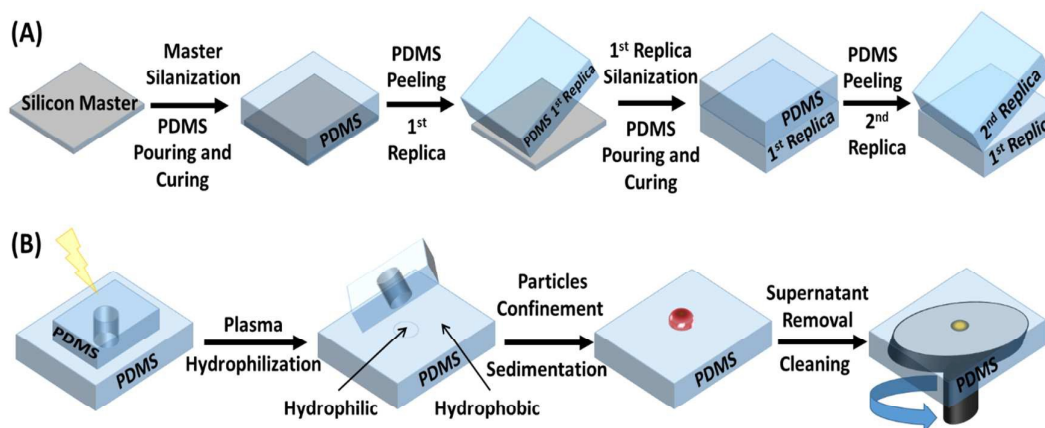
<sup>b</sup> Medcom Advance, Viladecans Business Park - Edificio Brasil, Bertran i Musitu 83 - 85, 08840 Viladecans - Barcelona, Spain. Email: [npazos@medcomadvance.com](mailto:npazos@medcomadvance.com)

<sup>c</sup> Leibniz Institut für Polymerforschung Dresden, e.V., Institute of Physical Chemistry and Polymer Physics, Hohe Str. 6, D-01069 Dresden, Germany.

<sup>d</sup> Departamento de Química Física e Inorgánica, Universitat Rovira i Virgili and Centro de Tecnologia Química de Catalunya, Carrer de Marcel·lí Domingo s/n, 43007 Tarragona, Spain. Email: [ramon.alvarez@urv.cat](mailto:ramon.alvarez@urv.cat)

<sup>e</sup> ICREA, Passeig Lluís Companys 23, 08010 Barcelona, Spain.

Electronic Supplementary Information (ESI) available: UV-Vis spectra and TEM and SEM images of different particles and supercrystals. See DOI: 10.1039/x0xx00000x



**Scheme 1.** Outlines of the (A) micro-structured template fabrication via replica molding; and (B) discrete microcrystals fabrication via confinement strategy based on the generation of a wetting contrast at the substrate surface.

**Materials and methods:** Ammonia solution (25%,  $\text{NH}_4\text{OH}$ ), hydrogen peroxide (30%), and isopropanol (99.9%) were purchased from VWR. Gold(III) chloride trihydrate (99.9%,  $\text{HAuCl}_4 \cdot 3\text{H}_2\text{O}$ ), trisodium citrate dehydrated ( $\geq 99.5\%$ ,  $\text{C}_6\text{H}_5\text{Na}_3\text{O}_7 \cdot 2\text{H}_2\text{O}$ ), 11-mercaptoundecanoic acid ( $\geq 95\%$ , MUA), Ethanol absolute ( $\geq 99.9\%$ , EtOH), and ascorbic acid (99.9%) were purchased from Sigma-Aldrich (Germany). N-cetyl-N,N,N-trimethylammonium bromide (99.72%, CTAB) was acquired from Merck. Poly(dimethyl siloxane) (PDMS) silicon elastomer (Sylgard 184 base and curing agent) were obtained from Dow Corning. Heptadecafluoro-1,1,2,2-tetrahydrodecyl dimethylchlorosilane was purchased from ABCR GmbH & Co. KG. Syringe filters were bought from Millipore. Teflon-coated silicon masters  $15 \times 15 \text{ mm}^2$  were purchased from HTS Resources. All reactants were used without further purification. Milli-Q water ( $18 \text{ M}\Omega \text{ cm}^{-1}$ ) was used in all aqueous solutions, and all the glassware was cleaned with *aqua regia* before usage.

**Synthesis of spherical gold nanoparticles:** CTAB-stabilized spherical gold nanoparticles of approx. 80 nm in diameter were produced according to a reported seed mediated procedure.<sup>18</sup> Briefly, seed particles were prepared by adding sodium citrate and  $\text{HAuCl}_4$  to 20 mL of water to achieve a final concentration of  $2.5 \times 10^{-4} \text{ M}$  for each reactant. Subsequently,  $\text{NaBH}_4$  (600  $\mu\text{L}$ , 0.1 M) was quickly injected meanwhile the solution was energetically stirred, (1200 rpm). Stirring was continued for 1h at open atmosphere to allow the  $\text{NaBH}_4$  to decompose avoiding over pressure. Immediately after addition of  $\text{NaBH}_4$  the color of the solution changed from colorless to red indicating the formation of gold particles. Next, a growth solution was prepared by dissolving CTAB in Milli-Q water (f.c. 0.1 M, 1000 mL). Followed by the addition of  $\text{HAuCl}_4$  (0.112 M, 4216  $\mu\text{L}$ ), NaI (0.1 mM, 138  $\mu\text{L}$ ) and ascorbic acid (0.1 M, 7350  $\mu\text{L}$ ). After each addition, the reaction vessel was vigorously shaken. Afterwards the solution was thermostated to 32 °C. Then 2300  $\mu\text{L}$  of the as prepared seeds were carefully added in the foam of the grow solution, the mixture was vigorously shaken and the bottles were left undisturbed at 32

°C for 48 h. After this time, sediment in the bottom of the flask is observed. In order to maximize nanoparticle monodispersity, the supernatant was carefully collected and the precipitate discarded. Based on SEM pictures, after sedimentation there is still remaining a small amount of bigger particles with different shapes, like rods and plates. With the aim to obtain a highly homogeneous system, the gold nanoparticles solution was then filtered (0.2  $\mu\text{m}$  pore size). The used syringe filters have PP housings, which contain hydrophobic PTFE membranes. The hydrophobic membrane was turned hydrophilic by rinsing it with Milli-Q water. Afterwards, gold colloids were centrifuged three times at 6000 rpm for 15 minutes. After each centrifugation step, the nanoparticles were redispersed using a 1 mM CTAB stock solution to assure that the final CTAB concentration was 1 mM. One last centrifugation step was necessary to adjust the concentration of the nanoparticles to 20 mg/mL. Moreover, citrate- and MUA- stabilized spherical gold nanoparticles of approx. 80 nm in diameter were produced. To prepare citrate stabilized particles,<sup>37</sup> 1540  $\mu\text{L}$  of an aqueous solution of  $\text{HAuCl}_4$  (0.081 M) was added to a boiling aqueous solution of sodium citrate (500 mL, 0.27 mM) under vigorous stirring. A condenser was used to prevent solvent evaporation. During this time (30 min), the color of the solution gradually changed from colorless to purple to finally become deep red. After that, the reaction was cooled down until the temperature of the solution reached 90 °C. Then, a sequential addition of sodium citrate and  $\text{HAuCl}_4$  was performed as follows. First, 4.0 mL of sodium citrate (0.1 M) were injected, 5 min after, 2 mL of sodium citrate (0.1 M) and 808.5  $\mu\text{L}$  of  $\text{HAuCl}_4$  (0.1 M) were sequentially injected (time delay approx.. 2 min) and the reaction was left under stirring at 90 °C for 30 min. This process was repeated 3 times to finally obtain Au NPs of approx. 80 nm. MUA stabilized Au particles were obtained by functionalizing 250 mL of the as-produced citrate gold nanoparticles with MUA (4 molecules/nm<sup>2</sup>). To this end, a solution containing  $\text{NH}_4\text{OH}$  (400  $\mu\text{L}$ , 2.9% aqueous solution) and MUA (470  $\mu\text{L}$ ,  $10^{-3} \text{ M}$  in EtOH) was prepared and added under vigorous stirring to the gold nanoparticle

solution. Agitation was continued for 90 min to ensure MUA functionalization of the Au surface. Next, the Au particles were cleaned by centrifugation at 6000 rpm for 15 minutes and redispersed in Milli Q water. Afterwards, both gold colloids (stabilized with citrate and MUA respectively) were centrifuged several times (x3) at 6000 rpm for 15 minutes to reach a final Au concentration of 20 mg/mL.

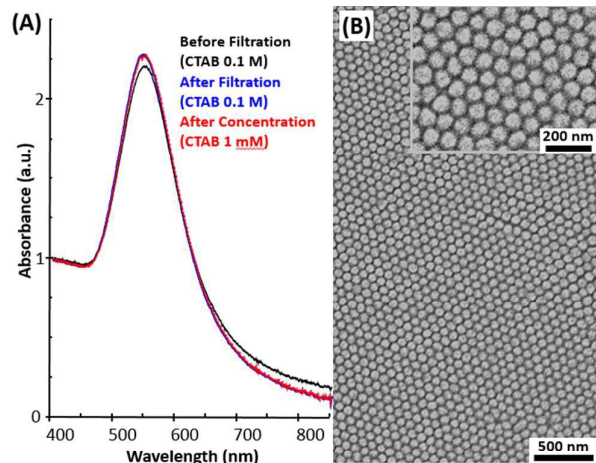


**Fig. 1.** (A) UV- vis spectra corresponding to Au NPs before and after filtration (black and blue curve, respectively) and after CTAB removal (red). (B) SEM images from the filtrated Au NPs.

**Replica molding:** Replicas from silicon masters with periodic patterns etched on its surfaces were produced with PDMS. In order to replicate three dimensional structures, fluid PDMS is poured over the silicon masters. Before the masters were casted with PDMS (25 g Sylgard 184 Base and 2.5 g Sylgard 184 curing agent, mixing ratio of 10: 1),<sup>38, 39</sup> the two PDMS components were mixed by stirring for 15 minutes. The substrates were cleaned with water, ethanol and toluene, from the polar solvent to the nonpolar solvent and then dried with N<sub>2</sub> stream. Shortly after pouring the masters with PDMS, the substrates were degassed in a desiccator for 2 h to remove any gas. After that, the PDMS was cured for another 2 h in the oven at 80°C under vacuum. Upon cooling the solid elastomeric PDMS were peeled off obtaining the first replication. Then the PDMS stamps were treated with O<sub>2</sub> plasma for 60 s to render them hydrophilic.<sup>40</sup> After that, the elastomeric stamps were silanized via gas phase deposition of heptadecafluoro 1,1,2,2 tetrahydrodecyl dimethylchlorosilane in a desiccator overnight. To clean the stamps from any excess of silane, they were cleaned again with toluene, ethanol, Milli-Q water and dried with N<sub>2</sub>. Subsequently, the first replicas were used as masters for the next replica molding step. The second replicas were manufactured following the replication steps previously reported for the first replica.

**Colloidal crystals:** All the crystal were produced using PDMS replicas of the silicon masters. The first step of the droplet confinement process is the preparation of a 1 cm x 1 cm

square of PDMS with a hole in the middle (3 mm diameter). The PDMS square with the hole, was placed on the structured PDMS replica as a mask to produce the hydrophilic confinement area. Subsequently the sample was treated with O<sub>2</sub> plasma for 180 s. Afterward, the PDMS square with the hole was removed. Then a 10 μL droplet of the concentrated GNP solution ([Au] = 20 mg/mL, [CTAB] 1 mM) was drop casted on the hydrophilic area of the plasma treated substrate. The whole setup was put in a humidity chamber to avoid evaporation of the solvent, enabling the particles to sediment. After the particles were sediment (24 h), the residual water was removed *via* spin coating at 2500 rpm for 100 s. Two additional cleaning steps were performed spin coating each time 60 μL of water at the same conditions. The system was dried with N<sub>2</sub> and the dried crystal was transferred to a glass substrate utilizing adhesive tape.

**Characterization:** UV-VIS spectroscopy was recorded with a PerkinElmer, Lambda 19. Size, shape and topographical characterization of the nanoparticles and their macroscale assemblies were characterized with transmission and scanning electron microscopy (TEM, LEO 922 EFTEM operating at 200 kV and LEO 1530 FE-SEM, Zeiss), and atomic force microscopy (AFM, NanoScope Dimension IIIIm NanoScope V, Veeco Metrology Group).

**SERS spectroscopy:** SERS spectra were collected in backscattering geometry with a Renishaw Invia Reflex system equipped with a 2D-CCD detector and a Leica confocal microscope. The spectrograph used a high resolution grating (1200 g cm<sup>-1</sup>) with additional band pass filter optics. Excitation of the sample was carried out with a 785 nm diode laser line, with acquisition times of 10<sup>-1</sup> s (depending on Raman Intensity saturation) and power at the sample of about 300 mW, using the Renishaw StreamLine accessory. The laser was focused onto the sample with a 100× objective (N.A. 0.9) providing a spatial resolution of ca. 0.5 μm and a laser penetration depth of ca. 0.3 μm (for gold materials of refractive index equals to 0.27049).<sup>41, 42</sup>

## Results and discussion

Successful NP assembly into densely packed and well-ordered three dimensional supercrystals requires the simultaneous control of different experimental parameters. First of all, colloidal nanoparticles must possess a narrow size distribution (<10% standard deviation).<sup>36</sup> Secondly, an external force such as gravity, magnetic or electric fields should be applied to the system to properly direct the particle assembly<sup>43</sup> since interparticle forces determining the colloidal equilibrium (i.e. van der Waals, Coulombic, dipolar etc.) cannot be exploited to dictate the self-assembly pathway. For nanoparticles made of high density materials such as gold, sedimentation then becomes an effective method for engineering NP assembly. For these reasons, we selected highly symmetric spherical gold NP of relatively large size (and weight) to fabricate our micro-structured crystals.

The synthesis of these colloids was performed by a cetyltrimethylammonium bromide (CTAB) assisted seeding growth process,<sup>18</sup> followed by a filtration step to eliminate potential aggregates. This protocol yields particles of ca. 80 nm diameter with a localized surface plasmon resonance (LSPR) centered at 548 nm (Fig. 1A).

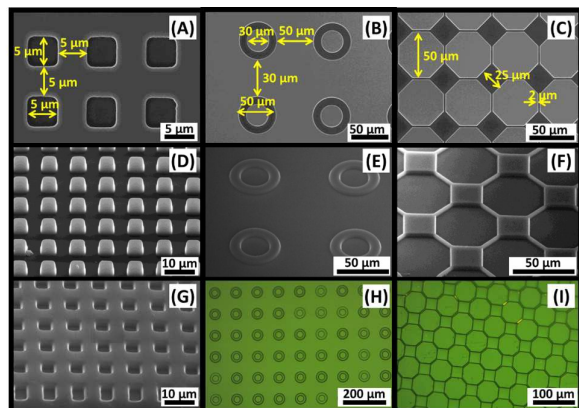


**Fig. 2.** SEM images of representative silicon masters used for replica molding (A, B, and C); 1st PDMS replicas (D, E, and F); and 2nd PDMS replicas (G). (H and I) are optical microscopy images of the 2nd PDMS replicas.

Nanoparticles spontaneously order into superlattices when their concentration exceeds a critical value.<sup>18</sup> Usually this is achieved by solvent evaporation during the crystal formation.<sup>19</sup> However, this procedure results in a continuous crystal film. To form discrete superlattices, pre-concentration of colloidal solutions is necessary. Thus, the initial colloidal NPs were repeatedly centrifuged to increase their final concentration up to 20 mg of gold per mL. Importantly, during these centrifugation cycles the CTAB concentration was progressively reduced from 0.1 M to 1 mM (i.e. the critical micellar concentration)<sup>44</sup> in order to remove the excess of surfactant in solution. This avoids the CTAB crystallization within the micro-structures, which leads to their disruption, while preserving the nanoparticle colloidal stability (i.e. no aggregation, Fig. 1B). It is worthy to note, that CTAB stabilized Au particles were selected because of their homogeneity and monodispersity. However, the presented method can also be successfully applied to nanoparticles with different surface stabilizers, such as citrate and 11-mercaptoundecanoic acid (MUA). In this regard, Figure 1S shows the UV-vis and TEM characterization of the Au particles in solution stabilized either with citrate or MUA, while Figure 2S shows their corresponding supercrystals.

**Scheme 1** depicts the entire procedure for the fabrication of discrete colloidal crystals. In the first step, the appropriate micro-structured template is prepared via replica molding (**Scheme 1A**). It is possible to assemble NPs directly on topographically patterned silicon masters<sup>19</sup> but such masters are very expensive to produce and their reutilization capacity

is limited. Besides, their use encompasses severe difficulties, especially regarding of their handling during crystal formation and deposition. To overcome these problems, replica molding (REM) was used as an efficient alternative to replicate surface topography.<sup>45-49</sup> This technique enables the replication of

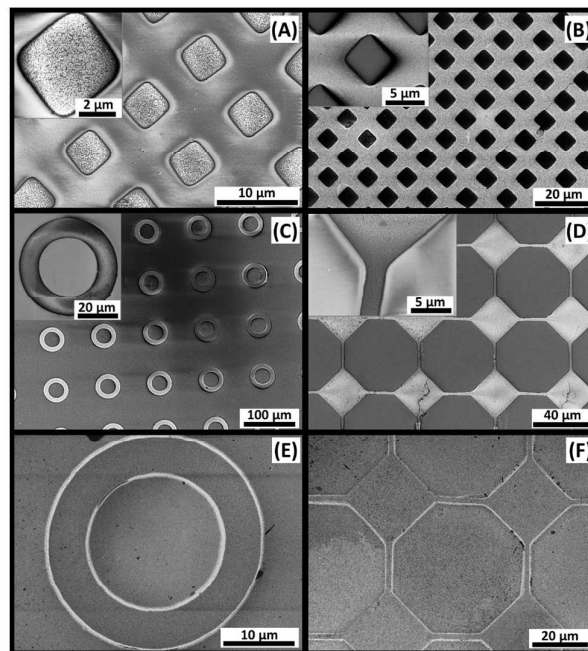


**Fig. 3.** SEM images of some representative supercrystals: (A) cubes, (B) square-like grids, (C) rings and (D) cubes linearly connected between them through their edges. (E) and (F) illustrates some structures where no spin-coating was performed, showing the presence of an evident continuous layer of particles underneath the microstructures.

three dimensional structures in a single step,<sup>39, 46</sup> allowing the use of expensive silicon masters, manufactured by conventional optical or electron beam lithography, as templates for molding elastomeric substrates with curable polymers without damaging the original masters. These molds can be reused multiple times to produce colloidal crystals. An important issue during the REM process is the fidelity of the replicas to the original template.<sup>45</sup> This is influenced by many factors like van der Waals-forces or the wetting properties at the template/polymer interface.<sup>39, 46</sup> Keeping this in mind, polydimethylsiloxane (PDMS) was selected as the elastomer because of its low interfacial free energy (21.6 dyn/cm),<sup>39</sup> and its good chemical and thermal stability (up to 186 °C).<sup>39</sup> In addition, surface wetting properties of PDMS can be easily tuned from hydrophobic to hydrophilic.<sup>32</sup> This is particularly important for the crystal formation process since a good wettability is required so that NPs can fill the template grooves as described by the so-called Wenzel state.<sup>17, 50</sup>

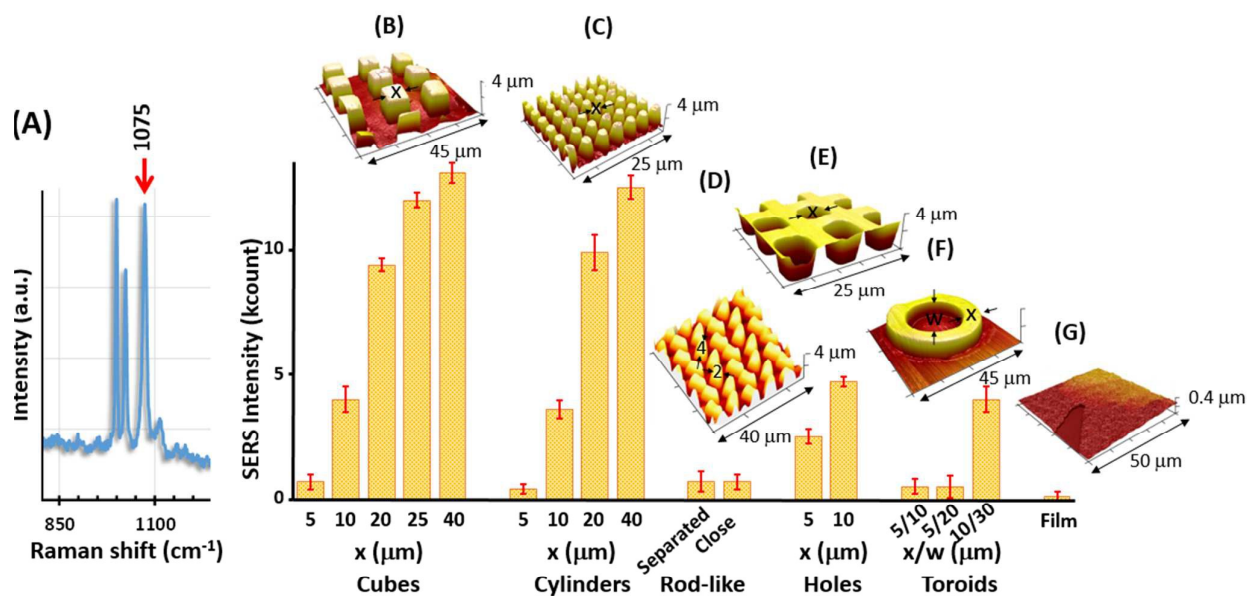


**Fig. 4.** (A) SERS spectrum of benzethiol (BT) on gold in the 840–1200  $\text{cm}^{-1}$  spectral region. (B–G) SERS intensity of the 1075  $\text{cm}^{-1}$  BT band on supercrystals with different geometries (B) cubic, (C) cylindrical, (D) rod-like, (E) holes, (F) toroidal and (G) film) and with different dimensions.

To exactly replicate the silicon masters, two different replica moldings are necessary. The first one provides the negative structure of the silicon stamp, and is prepared by casting (PDMS is cured onto the silanized silicon masters). The second molding is obtained by using the same fabrication protocol but in this case the polymer is cured onto the negative PDMS pattern, thus yielding the equivalent positive pattern of the initial silicon master (**Scheme 1A**). Importantly, the negative PDMS master is previously treated with heptadecafluoro-1,1,2,2-tetrahydrodecyl dimethylchlorosilane to avoid the cross-linking of the master silanol groups with those of the new PDMS.<sup>51–53</sup> This treatment also facilitates a long-lasting hydrophobization of the surface.<sup>32</sup> The silicon masters used in this work and their corresponding negative and positive PDMS replicas are shown in **Fig. 2** (A,B,C are silicon masters; D,E,F are 1<sup>st</sup> PDMS replicas; and G, H, I are 2<sup>nd</sup> PDMS replicas).

In addition to the right substrate wettability (hydrophilic) and a high particle concentration, a third requirement for supercrystals formation is the confinement of the NPs into the structure of the master. Although the use of physical barriers is suitable to avoid the dispersion of the NPs over the whole surface,<sup>19</sup> this physical entrapment does not allow the removal of the excess neither of particles nor of the surfactant. In particular, CTAB can sediment and crystallize on the template, inhibiting the organization of the NPs into individual microstructures. Thus, for the fabrication of discrete microcrystals we developed a new confinement strategy based on the generation of a wetting contrast at the substrate surface. The wetting properties of the PDMS surface can be changed from hydrophobic to hydrophilic via plasma treatment. Thus, as illustrated in **Scheme 1B**, hydrophilization

of a defined area of the templating substrate was carried out by depositing a mask with a circular hole (3 mm in diameter) on the PDMS master. A subsequent oxygen plasma treatment selectively generates a local area of temporal hydrophilicity, corresponding to the exposed surface of the PDMS mask. Such induced wetting contrast between the confined hydrophilic area and the surrounding hydrophobic surface allows to selectively confine the aqueous NP droplet in the hydrophilic region.

Slow organization of the nanoparticles into the supercrystal is then achieved via a sedimentation process driven by gravitational and capillary forces.<sup>18, 19</sup> To avoid solvent evaporation and, thus, surfactant crystallization within the solution, the samples were placed in a humidity chamber (95% humidity) with controlled temperature (27 °C) during the sedimentation step. Once the nanoparticle deposition is completed, the excess of NP is removed from the structured surface via spin-coating (**Scheme 1B**), which also contributes in lowering the overall surfactant concentration (i.e. CTAB is eliminated with the residual water). Finally, after the drying process is terminated, the crystals form a superlattice in which they are held together by strong cohesive interactions between neighbouring ligands and nanocrystals.<sup>19</sup> The crystals can then be transferred to any surface (e.g. glass slides) by simply using adhesive tape. **Fig. 3 A–D** illustrates some examples of well-controlled assemblies of discrete colloidal crystals on glass slides including cubes, holes, toroids or connected cubes. The figure also illustrates some structures where no spin-coating was performed, showing the presence of an evident continuous layer of particles underneath the microstructures (**Fig. 3E and F**).

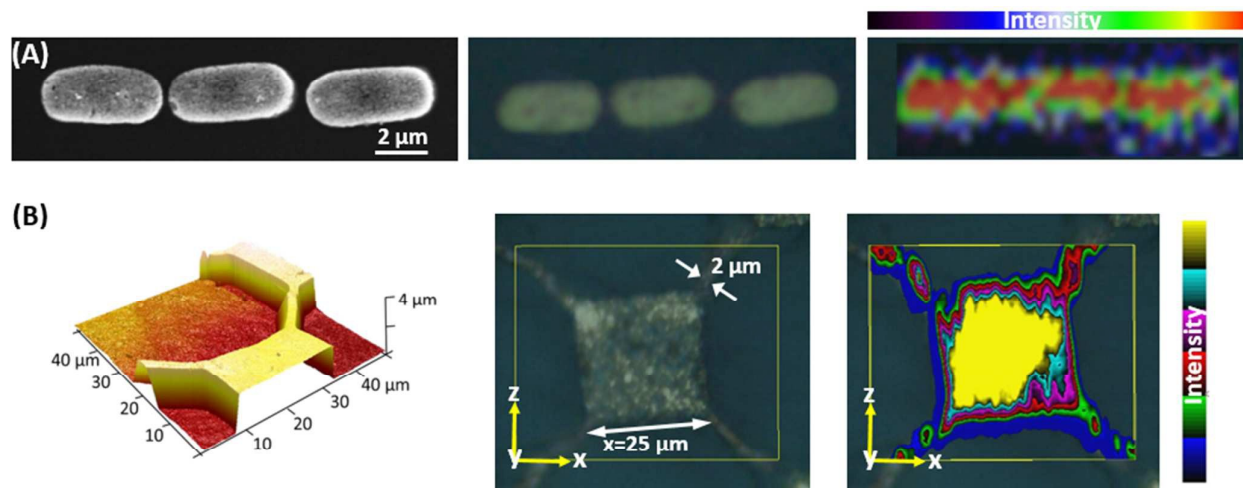


**Fig. 5.** (A) SEM, white light and SERS images of rod-like supercrystals in close proximity. (B) Representative 3D AFM image of a complex supercrystal and their optical and SERS images in the  $xz$  plane.

The reusability of the PDMS templates was also investigated. We observed that Millipore water rinsing in combination with ultrasound for 5 minutes is sufficient to regenerate cleaned PDMS templates. However, a more intense treatment might be recommended to guarantee a perfect cleaning. For instance, we used a combination of different rinsing steps with toluene, ethanol and water in combination with ultrasound. In any case, special care should be taken during such cleaning cycles, since organic solvents are known to induce PDMS swelling. Additional short cleaning steps with *aqua regia* rapidly followed by thorough rinsing with Millipore water can be also included.

In order to test the optical enhancing properties through SERS, the colloidal crystals were exposed to an  $O_2$  plasma to remove all residual organics from the metallic surfaces, including CTAB.<sup>17</sup> Then a monolayer of benzenethiol (BT), selected as the Raman probe, was deposited in gas phase on the substrates. **Fig. 4A** shows the characteristic SERS fingerprint of BT on gold surfaces in the  $840\text{--}1200\text{ cm}^{-1}$  spectral region. SERS characterization of crystals with different morphological features was carried out using a near infrared (785 nm) laser and the intense BT band at  $1075\text{ cm}^{-1}$  was selected as the spectral marker to map the SERS intensity (**Fig. 4B**). It is worthy to note that although the side dimensions of the crystal were varied, the height ( $y$ ) was maintained constant at  $4\text{ }\mu\text{m}$ . For comparison, spectra were also recorded on the surface of a regular continuous nanoparticle film ( $0.3\text{ }\mu\text{m}$  height, **Fig. 4B**). Since the film height is much larger than the laser penetration depth (estimated at  $0.3\text{ }\mu\text{m}^{41}$ ), the differences in absolute SERS intensity represented in **Fig. 4** can be directly ascribed to the collective properties of the supercrystals (i.e. the overall SERS signals are generated by approximately the same number of nanoparticles and, thus, of Raman molecules). Several remarkable features arise from the analysis of the SERS mapping. First, all the patterned substrates provide a

consistent larger intensity than that sustained by the continuous film. Second, independently of the material geometry, the absolute intensity increases as the side  $x$  of the supercrystal increases, giving rise to similar enhancements for similar  $x$  values (see, for example cubes and toroids of  $5$  or  $10\text{ }\mu\text{m}$ ).

Intrigued by these observations, we further designed two new experiments. In the first one, SERS signals derived from rod-like organized supercrystals separated by gaps in between  $2$  and  $4\text{ }\mu\text{m}$  (**Fig. S3**) were compared with closely spaced similar structures (**Fig. 5A**). Notably, the SERS response was similar both in distribution and in intensity (**Fig. 4E** and **5A**). This experiment suggests that supercrystal field intercoupling is negligible due to the much larger interaction within the individual complex structure. In the second experiment, a new geometrically complex supercrystal obtained by combining cubes of  $25\text{ }\mu\text{m}$  side interconnected by  $2\text{ }\mu\text{m}$  side lines, was investigated to study the optical signals under the exactly same circumstances. Once more, the height of the whole construct was kept constant at  $4\text{ }\mu\text{m}$  (**Fig. 5B**). The SERS image of the  $xz$  plane displays a gradient of intensities that decreases from the center to the edges of the crystal. The connecting lines in between the cubes show a considerably smaller intensity as compared with the large crystal. Such result contrasts with what it is expected from pure plasmonic interacting nanostructures. In that case, generation of hot spots of analogous geometry and particle number would yield similar SERS enhancements.

Due to the dimensions of the supercrystals and considering that the wavelength of the incident light is approximately one order of magnitude larger than the size of the nanoparticle building block, we cannot assume a generation of strong cavity modes. However, a possible explanation for the outcome of the SERS map can be related to generation of some kind of

standing waves that co-add enhancement to the canonical hot spots.<sup>54</sup>

In fact, this situation, has been theoretically demonstrated before for closely-packed planar metallic nanoparticle arrays which host strongly-bound transverse electric surface waves that are more confined than surface plasmon polaritons with the subsequent increase in the surface electric field and, thus, in the SERS intensity by over one order of magnitude.

## Conclusions

In summary, we have developed a new method for the massive fabrication of discrete nanoparticle supercrystals with complex geometries. These plasmonic supercrystals generate and additional electric response, upon illumination with NIR light, that generate an extra optical enhancement additive to that of the LSPRs typical of plasmonic clusters of nanoparticles. All these features have a deep impact in the surface electric field generated by the optical substrates and, thus, in their optimal design for real applications such as SERS substrates.

## Acknowledgements

This work was funded by the Spanish Ministerio de Economía y Competitividad (CTQ2014-59808R), the Generalitat de Catalunya (2014-SGR-480), the European Research Council (PRIOSERS FP7MC-IEF-623527, and METAMECH, ERC-StG 306686) and by Medcom Advance SA. We are grateful for the fruitful discussion with Professor Javier Garcia de Abajo from ICFO.

## Notes and references

1. T. Kraus, D. Brodoceanu, N. Pazos-Perez and A. Fery, *Adv Funct Mater*, 2013, **23**, 4529-4541.
2. A. Stein and R. C. Schroden, *Curr Op Colloid Interface Sci*, 2001, **5**, 553-564.
3. O. D. Velev and S. Gupta, *Adv Mater*, 2009, **21**, 1897-1905.
4. X. Zhang, J. Zhang, Z. Ren, X. Li, X. Zhang, D. Zhu, T. Wang, T. Tian and B. Yang, *Langmuir*, 2009, **25**, 7375-7382.
5. F. Ç. Cebeci, Z. Wu, L. Zhai, R. E. Cohen and M. F. Rubner, *Langmuir*, 2006, **22**, 2856-2862.
6. Y. Lu, G. L. Liu, J. Kim, Y. X. Mejía and L. P. Lee, *Nano Lett*, 2005, **5**, 119-124.
7. C. Sun, L.-Q. Ge and Z.-Z. Gu, *Thin Solid Films*, 2007, **515**, 4686-4690.
8. K. Liu and L. Jiang, *Ann Rev Mater Res*, 2012, **42**, 231-263.
9. W.-L. Min, B. Jiang and P. Jiang, *Adv Mater*, 2008, **20**, 3914-3918.
10. Y. Li, J. Zhang and B. Yang, *Nano Today*, 2010, **5**, 117-127.
11. C. Werderius, L. Österlund and B. Kasemo, *Langmuir*, 2003, **19**, 458-468.
12. B. Wickman, Y. E. Seidel, Z. Jusys, B. Kasemo and R. J. Behm, *ACS Nano*, 2011, **5**, 2547-2558.
13. C. M. Soukoulis and M. Wegener, *Nat Photon*, 2011, **5**, 523-530.
14. O. Benson, *Nature*, 2011, **480**, 193-199.
15. O. D. Velev and A. M. Lenhoff, *Curr Op Colloid Interface Sci*, 2000, **5**, 56-63.
16. C. Burda, X. Chen, R. Narayanan and M. A. El-Sayed, *Chem Rev*, 2005, **105**, 1025-1102.
17. R. A. Alvarez-Puebla, A. Agarwal, P. Manna, B. P. Khanal, P. Aldeanueva-Potel, E. Carbó-Argibay, N. Pazos-Pérez, L. Vigderman, E. R. Zubarev, N. A. Kotov and L. M. Liz-Marzán, *Proc Nat Acad Sci USA*, 2011, **108**, 8157-8161.
18. N. Pazos-Perez, F. J. Garcia de Abajo, A. Fery and R. A. Alvarez-Puebla, *Langmuir*, 2012, **28**, 8909-8914.
19. M. Alba, N. Pazos-Perez, B. Vaz, P. Formentin, M. Tebbe, M. A. Correa-Duarte, P. Granero, J. Ferré-Borrull, R. Alvarez, J. Pallares, A. Fery, A. R. de Lera, L. F. Marsal and R. A. Alvarez-Puebla, *Angew Chem Int Ed*, 2013, **52**, 6459-6463.
20. L. Xu, W. Ma, L. Wang, C. Xu, H. Kuang and N. A. Kotov, *Chem Soc Rev*, 2013, **42**, 3114-3126.
21. X. Ye, J. Chen and C. B. Murray, *J Am Chem Soc*, 2011, **133**, 2613-2620.
22. X. Ye, L. Jin, H. Caglayan, J. Chen, G. Xing, C. Zheng, V. Doan-Nguyen, Y. Kang, N. Engheta, C. R. Kagan and C. B. Murray, *ACS Nano*, 2012, **6**, 2804-2817.
23. O. Hess, J. B. Pendry, S. A. Maier, R. F. Oulton, J. M. Hamm and K. L. Tsakmakidis, *Nat Mater*, 2012, **11**, 573-584.
24. M. L. Brongersma and V. M. Shalaev, *Science*, 2010, **328**, 440-441.
25. S. Lal, S. Link and N. J. Halas, *Nat Photon*, 2007, **1**, 641-648.
26. N. Pazos-Perez, W. Ni, A. Schweikart, R. A. Alvarez-Puebla, A. Fery and L. M. Liz-Marzan, *Chem Sci*, 2010, **1**, 174-178.
27. A. Guerrero-Martinez, J. Perez-Juste, E. Carbo-Argibay, G. Tardajos and L. M. Liz-Marzan, *Angew Chem Int Ed*, 2009, **48**, 9484-9488.
28. S. Gomez-Grana, J. Perez-Juste, R. A. Alvarez-Puebla, A. Guerrero-Martinez and L. M. Liz-Marzan, *Adv Opt Mater*, 2013, **1**, 477-481.
29. Y. Jiao, D. Han, Y. Ding, X. Zhang, G. Guo, J. Hu, D. Yang and A. Dong, *Nat Commun*, 2015, **6**.
30. P. V. Kamat, *J Phys Chem C*, 2008, **112**, 18737-18753.
31. C.-F. Chen, S.-D. Tzeng, H.-Y. Chen, K.-J. Lin and S. Gwo, *J Am Chem Soc*, 2008, **130**, 824-826.
32. C. Hanske, M. B. Müller, V. Bieber, M. Tebbe, S. J Essl, A. Wittmann and A. Fery, *Langmuir*, 2012, **28**, 16745-16750.
33. T. Thai, Y. Zheng, S. H. Ng, S. Mudie, M. Altissimo and U. Bach, *Angew Chem Int Ed*, 2012, **51**, 8732-8735.
34. C. Hanske, M. Tebbe, C. Kuttner, V. Bieber, V. V. Tsukruk, M. Chanana, T. A. F. König and A. Fery, *Nano Lett*, 2014, **14**, 6863-6871.
35. C. Hamon, S. Novikov, L. Scarabelli, L. Basabe-Desmonts and L. M. Liz-Marzán, *ACS Nano*, 2014, **8**, 10694-10703.
36. D. V. Talapin, J.-S. Lee, M. V. Kovalenko and E. V. Shevchenko, *Chem Rev*, 2010, **110**, 389-458.
37. N. G. Bastús, J. Comenge and V. Puntès, *Langmuir*, 2011, **27**, 11098-11105.
38. Z. Almutairi, C. L. Ren and L. Simon, *Colloids Surf A*, 2012, **415**, 406-412.
39. D. Qin, Y. Xia and G. M. Whitesides, *Nat. Protocols*, 2010, **5**, 491-502.
40. D. Bodas and C. Khan-Malek, *Sensor Act B*, 2007, **123**, 368-373.
41. R. A. Alvarez-Puebla, *J Phys Chem Lett*, 2012, **3**, 857-866.
42. M. Chen, I. Y. Phang, M. R. Lee, J. K. W. Yang and X. Y. Ling, *Langmuir*, 2013, **29**, 7061-7069.
43. Y. Min, M. Akbulut, K. Kristiansen, Y. Golan and J. Israelachvili, *Nat Mater*, 2008, **7**, 527-538.

44. S. Javadian, V. Ruhi, A. Heydari, A. Asadzadeh Shahir, A. Yousefi and J. Akbari, *Ind Eng Chem Res*, 2013, **52**, 4517-4526.
45. T. W. Lee, O. Mitrofanov and J. W. P. Hsu, *Adv Funct Mater*, 2005, **15**, 1683-1688.
46. X.-M. Zhao, Y. Xia and G. M. Whitesides, *J Mater Chem*, 1997, **7**, 1069-1074.
47. A. L. Thangawng, M. A. Swartz, M. R. Glucksberg and R. S. Ruoff, *Small*, 2007, **3**, 132-138.
48. T. Ohzono, H. Monobe, N. Fukuda, M. Fujiwara and Y. Shimizu, *Small*, 2011, **7**, 506-513.
49. G. Zhang, J. Zhang, G. Xie, Z. Liu and H. Shao, *Small*, 2006, **2**, 1440-1443.
50. R. N. Wenzel, *Ind Eng Chem*, 1936, **28**, 988-994.
51. V. Anand, S. Ghosh, M. Ghosh, G. M. Rao, R. Railkar and R. R. Dighe, *App Surf Sci*, 2011, **257**, 8378-8384.
52. I. Yilgor, S. Bilgin, M. Isik and E. Yilgor, *Polymer*, 2012, **53**, 1180-1188.
53. J. L. Fritz and M. J. Owen, *J Adhesion*, 1995, **54**, 33-45.
54. R. Sainidou and F. J. Garcia de Abajo, *Opt Exp*, 2008, **16**, 4499-4506.

TOC:

